Integrated Silicon-on-Insulator Spectrometer With Single Pixel Readout for Mid-Infrared Spectroscopy

Anton Vasiliev ⑩, *Student Member, IEEE*, Muhammad Muneeb, Jeroen Allaert,
Joris Van Campenhout, *Member, IEEE*, Roel Baets ⑩, *Fellow, IEEE*, and
Günther Roelkens ⑩, *Senior Member, IEEE*

Abstract—**Mid-infrared spectroscopy in the 2–4 μm wavelength range is of cardinal value for many sensing applications. Current solutions involve bulky and expensive systems to operate. Silicon-on-Insulator (SOI) waveguide technology offers means to miniaturize the different parts of the spectrometer. However, the development of on-chip detectors for the mid-infrared wavelength range is in its infancy and the characteristics are not on par with their discrete (cooled) counterparts. In this work, a compact and cheap mid-infrared spectrometer is realized by integrating a SOI arrayed waveguide grating (AWG) spectrometer operating in the 2.3 μm wavelength range with a high performance mid-infrared photodiode. The AWG has 12 output channels with a spacing of 225 GHz (4 nm) and a free spectral range of 3150 GHz (56 nm), which are simultaneously collected by a single, transistor outline (TO)-packaged extended InGaAs PIN photodiode. The response of each AWG channel is discerned by time-sequentially modulating the optical power in each output channel using integrated Mach-Zehnder based thermo-optic modulators with a π-phase shift power consumption of $\approx$50 mW. As an example, the absorption spectrum of a 0.5 mm thick polydimethylsiloxane sheet is sampled and compared to a benchtop spectrometer to good agreement.**

Index Terms—**Infrared spectroscopy, integrated optoelectronics, optical spectroscopy, silicon on insulator (SOI) technology, spectroscopy.**

I. INTRODUCTION

SILICON photonics has been tremendously successful in the area of optical communication [1]–[4]. The main reason is that the Silicon-on-Insulator (SOI) platform can benefit from well-established silicon electronics processes to manufacture photonic devices in high volumes and high yield but at a low cost [5]. More over, the high refractive index contrast of SOI optical waveguides allows for a very tight bend radius and therefore, ultra compact devices can be fabricated. The portfolio of SOI waveguide technology applications has expanded towards applications such as bio-sensing [6]–[8],

biomedical analysis [9], [10], structural analysis [11], [12] and gas sensing [13], [14]. Over the years, there has been progressively more interest towards longer wavelengths for a variety of new sensing markets and in particular for mid-infrared absorption spectroscopy. It is well-known that gas molecules have strong rovibrational resonances in the mid-infrared (>2 μm) wavelength range [15]. It is possible to access these longer wavelengths (2–4 μm) in the same SOI waveguide platform without leaving the well-established CMOS fabrication technology. However, this transition requires careful redesign of all the different subcomponents at these wavelengths [16]–[19]. The realization of silicon photonics components in this wavelength range could enable economical and compact optical sensors with superior performance in sensitivity, power consumption and portability compared to current bulky solutions. The absorption of SiO_2 beyond 4 μm wavelength and the substrate leakage set the upper wavelength limit for traditional SOI waveguide technology [16], [20], [21].

There are several approaches to realize a compact and cheap spectroscopic system and the required wavelength coverage and resolution determine the best solution. For spectroscopy of gases, a high resolution spectrum in a narrow wavelength range is typically required. This can be realized with mid-infrared distributed feedback (DFB) laser sources which can be thermally tuned over a narrow wavelength range [22]–[24]. The wavelength range can be further increased by fabricating an array of DFB lasers with slightly different central wavelengths. The central wavelength of each DFB laser can be adjusted by small alterations in the design [25]. The output from such a laser array could be multiplexed to a single diffraction limited output beam with low loss by using a high-performance SOI wavelength (de)multiplexer (WDM) such as an Arrayed Waveguide Grating (AWG) or Planar Concave Grating (PCG) [26], [27].

For spectroscopy applications involving broad absorption features such as liquids and solids where wavelength coverage is more important than resolution, a more cost-efficient solution including a broadband light source and a dispersive element is more suitable. Substantial effort is devoted to develop such novel spectrometers that are compact and can be integrated with photonic ICs. Some examples include spatial heterodyne spectrometers (SHS) [28], on-chip microelectromechanical (MEMS)-based Fourier Transform Infrared Spectrometers (FTIR) [29], stationary FTIRs [30] and AWGs [31]. The AWG is a versatile component for spectroscopy which can easily be
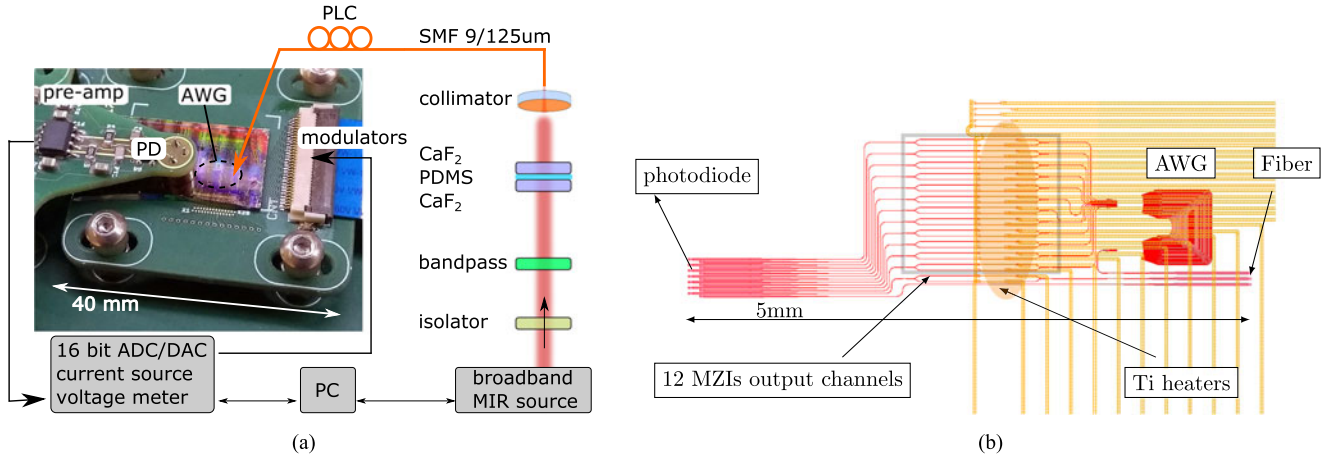
Fig. 1.   Schematic of the spectroscopy setup using a SOI AWG spectrometer with a single external detector (a). A Cr^{2+}: ZnS laser working in ASE mode with a bandpass filter is used as the broadband mid-infrared source to determine the absorption spectrum of a 0.5 mm thick PDMS sheet, held between two CaF_2 windows. The light is coupled to a standard 9/125 fiber pigtail. The TO-can with the photodiode is positioned directly on top of the output grating couplers of the chip and collects all twelve output channels of the AWG simultaneously. Design layout of the AWG (b). The output channels are modulated time-sequentially using (balanced) MZI thermo-optic modulators. A π-phase shift in each channel is achieved by dissipating $\approx$50 mW in the metal (Ti/Au) resistors placed 0.9 μm above the optical waveguide. The bandpass filter, PDMS and PD are not used in the passive characterization of the grating coupler efficiency and AWG response. Instead, a second single mode fiber is used to collect the output light and a mid-IR OSA is used as a sensitive power- and wavelength meter.

designed with good performance. The free spectral range (FSR) and channel spacing can be tailored to fit the application [32].

It is possible to heteregeneously integrate III-V-on-Silicon detectors on the photonic IC with the spectrometer in the 2–4 μm wavelength range [31], [33]. However, existing packaged (cooled) mid-infrared photodetectors currently outperform the on-chip solutions. We present an approach for integrating a single standard TO-can packaged InGaAs PIN photodiode with a twelve channel AWG with 225 GHz (4 nm) channel spacing. In order to distinguish the different channels, the output arms of the AWG are modulated using on-chip balanced Mach-Zehnder interferometers (MZIs) by thermal tuning [34]. To showcase the mini-spectrometer, the absorption spectrum of polydimethylsiloxane (PDMS) in the 2.3 μm wavelength range is recovered.

II. FABRICATION

The AWG is fabricated on a 200 mm SOI wafer with a 400 nm thick crystalline Si device layer and 2 μm buried oxide layer thickness. Rib waveguides and grating couplers (GCs) are defined with a 180 nm deep etch and are cladded with SiO_2 and planarized down to the silicon device layer. A thin 0.9 μm layer of SiO_x is deposited on top. 100/10 nm thick Ti/Au resistors are defined on the arms of the modulators. The resistors measure $200 \times 2 \ \mu m^2$ and realize a π-phase shift with $\approx$50 mW of power dissipation. As a final step, the chip is passivated with a benzo-cyclobutene (BCB) polymer layer. The circuit is designed for 2.3 μm wavelength and TE polarized light. The AWG has twelve channels with 225 GHz (4 nm) channel spacing and an FSR of 3150 GHz (56 nm). The MZI modulators of the photonic chip are wire bonded to a printed circuit board (PCB) and are addressed by a home-built 16-bit current source through USB. An uncooled Hamamatsu G12183-010K PIN photodiode (PD) is fixed to a pre-amplifier PCB with a variable gain up to 10^6 V/A. The electronics to drive the modulators and read the photodiode response

are based on off-the-shelf components. The PD is manually positioned and fixed 0.5 mm above the output grating coupler array of the AWG, see Fig. 1(a). The output grating array covers an area of $300 \times 140 \ \mu m^2$ and all the channels are simultaneously collected by the photosensitive area of the PD, 1 mm in diameter. The PD response is read-out using the aforementioned 16-bit ADC. A microcontroller is programmed to send the read/write commands in blocks with a resulting PD sampling rate of approximately 24 kSa/s. A 0.5 mm thick PDMS foil was prepared using the Sylgard 184 (10:1) elastomer kit and a suitable mold.

III. AWG CHARACTERIZATION

The performance of the photonic circuit is characterized using a Continuous Wave (CW) single mode Cr^{2+}:ZnS solid state laser from IPG Photonics. The free space output power from the laser is coupled to a standard 9/125 single mode fiber as in Fig. 1(a) but without the bandpass filter, PDMS and PD. The power in the fiber is between one and few tens of mW depending on the laser wavelength. A second single mode fiber collects the output light from the IC and a Yokogawa AQ6375 Optical Spectrum Analyzer (OSA) was used as a sensitive detector and wavelength meter. A cooled extended InGaAs PDA10DT photodetector from Thorlabs was used as a reference, connected to a 1/99 fiber splitter to compensate for slow time-fluctuations of the laser power. The AWG response with the MZI modulator arms is normalized to a reference waveguide and the results are shown in Fig. 2(a). The channel spacing is 225 GHz (4 nm) and one FSR spans 3150 GHz (56 nm). The insertion loss is around 2 dB and the crosstalk between channels is 20 dB. The grating coupler efficiency is calculated to be around -9 dB/GC at 2340 nm peak wavelength with 18 degrees fiber coupling angle, see Fig. 2(b). By switching the output fiber with the single pixel PD, the combined response of the AWG channels is retrieved. The PD voltage is normalized
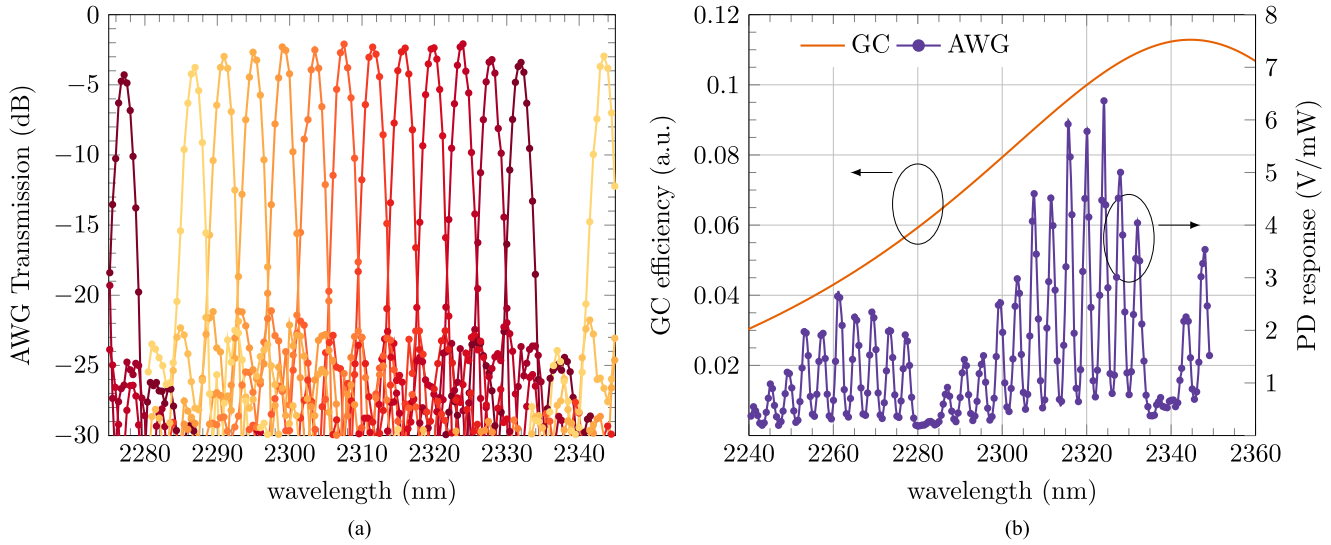
Fig. 2. The AWG channels from layout Fig. 1(b) are characterized using a single-mode tunable CW laser and normalized to a reference waveguide (a). The channel spacing is 225 GHz (4 nm) and one FSR spans 3150 GHz (56 nm). The insertion loss is around 2 dB and the crosstalk between channels is 20 dB. The output light is collected with a single mode fiber and the power and wavelength are obtained with the Yokogawa OSA. The grating coupler efficiency is estimated from the reference waveguide measurement (b). The insertion loss is 9 dB at 2340 nm peak wavelength and 18 degrees fiber coupling angle. The AWG response, normalized to the optical power in the fiber, is obtained from all channels simultaneously by using the TO-can PD as the detector. The PD response follows the GC efficiency curve and all twelve channels are visible. An additional envelope is observed due to limited dimensions and exact position of the PD on top of the output GC array. The beams coming from the edges of the output array are captured less efficiently. The position of the PD is fixed with screws but can be readjusted if needed.

to the power in the fiber towards the chip, calculated using the laser source reference detector. All twelve channels are clearly distinguishable. The combined AWG response follows the grating coupler trend with an additional envelope. The relative position of the output GC array to the PD and the finite aperture of the PD determine this envelope, see also Fig. 1. When the PD is positioned in the center of the GC array, the outer channels are captured less efficiently. The position of the PD is fixed with M4 screws and can be readjusted along x- and y-slits.

The MZI modulators are characterized using the same method as above but now the wavelength is fixed to the peak transmission of the AWG channel and electrical power is dissipated through the resistor on one of the arms of the MZI. The increased local temperature of the Si waveguide induces a change in effective index through the thermo-optic effect. The applied voltage and power are set with a Keithley 2400 measurement unit, see Fig. 3(a). The resistance is approximately 1200 Ω for all heaters and the extinction ratio is more than 30 dB. A π-phase shift is obtained when $P_\pi = 49$ mW power is dissipated. In the spectroscopy experiment where all twelve channels are collected simultaneously by the PD, the dissipated heat P_π on one channel causes a drop of $1.5/1.68 \approx 11/12$ of the amplified PD response as expected, see inset in Fig. 3(a). Due to small variations in fabrication, P_π varies between 48–56 mW and the corresponding V_π between 6–7 V for the 12 channels of the AWG. The AWG channel transmission is shown when the heater is switched on $V = V_\pi$ and when it is off $V = 0$, see Fig. 3(b). The pitch between the MZI channels is 100 μm. No thermal cross-talk between adjacent channels was observed and therefore must be lower than the optical crosstalk of the AWG, see Fig. 2(a).

IV. ABSORPTION SPECTROSCOPY

To showcase the single pixel mini-spectrometer, the absorption spectrum of PDMS in the 2.3 μm wavelength region is probed using three different methods. First, the absorption spectrum is determined using the Agilent 680 FTIR spectrometer in transmission, see Fig. 4(a). The importance of the 2–3 μm wavelength range is indeed also valid in this case as can be seen from the increased absorption cross section as compared to the 1.5–2 μm wavelength range.

Secondly, the PDMS sheet is placed between two 4 mm thick CaF_2 windows in the beam path of the Cr^{2+}:ZnS laser operating in amplified spontaneous emission (ASE) mode. The fiber coupled power is measured by the mid-infrared Yokogawa OSA with 0.1 nm resolution both with (PDMS), and without (Ref) the PDMS sample. The measured total optical power is 11.5 μW and 31.4 μW, respectively. When PDMS is introduced in the beam path, the collimator has to be realigned to a new optimum. The spectrum shows spectral ripple due to residual thin film interference effects of the bandpass filter. The normalized FTIR transmission of the PDMS sample and the bandpass filter is also shown in Fig. 4(b).

Lastly, the AWG is used as a dispersive spectrometer to recover the response of PDMS at the AWG peak wavelengths, marked as black crosses on the top axis in Fig. 4(b). Ideally, the AWG response would be limited to within one FSR closest to the PDMS absorption feature. The available bandpass filter is centered at 2305 nm with a Full Width at Half Maximum (FWHM) of 50 nm and overlaps unintentionally with the next FSR on the blue side of the PDMS absorption peak. As a result, the longer wavelength channels of the AWG spectrometer will show additional crosstalk.
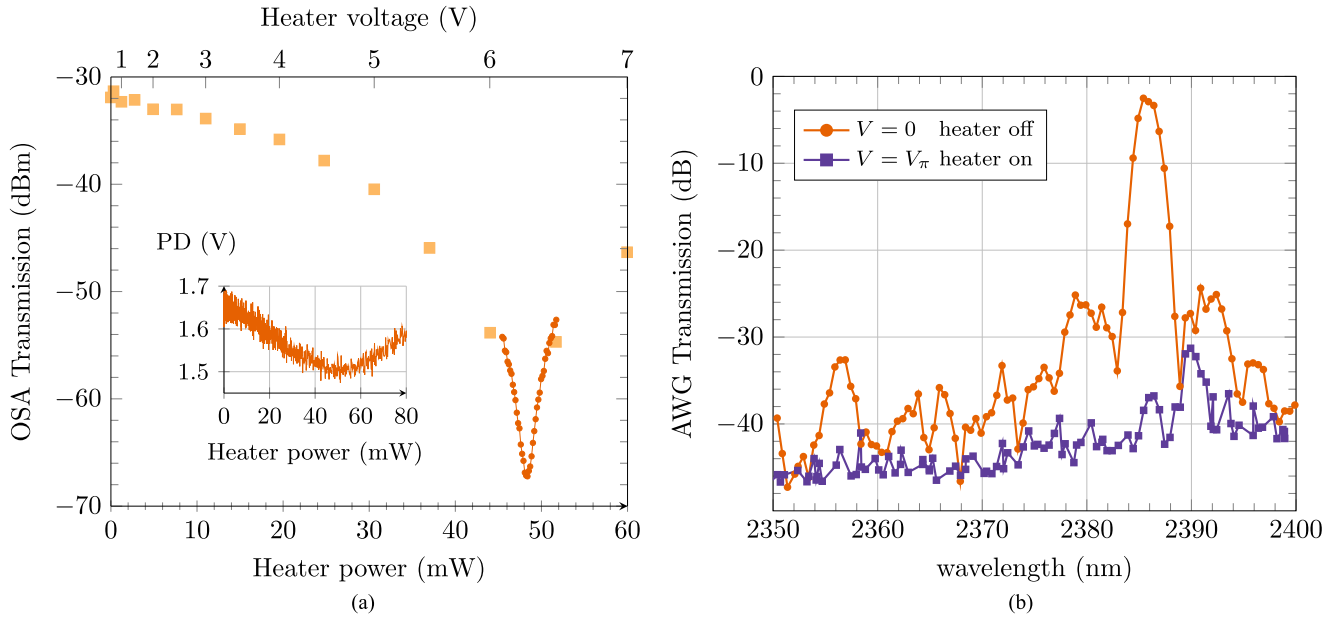
Fig. 3. The characterization of a MZI modulator as a function of dissipated power is shown for one channel of the AWG (a). A coarse and a fine voltage sweep is performed to find the minimum transmission of the channel at 2386 nm wavelength. The inset shows the amplified PD response as a function of dissipated heat on one channel when all twelve channels are collected simultaneously by the single pixel for the setup as in Fig. 1. The resistance is approximately 1200 Ω for all heaters and the extinction ratio of the MZI is more than 30 dB. A π-phase shift is obtained when $P_\pi = 49$ mW power is dissipated. Due to small variations in fabrication, P_π varies between 48–55 mW and the corresponding V_π between 6–7 V for the 12 channels of the AWG. The channel transmission is shown when the heater is switched on ($V = V_\pi$) and when it is off ($V = 0$) (b).
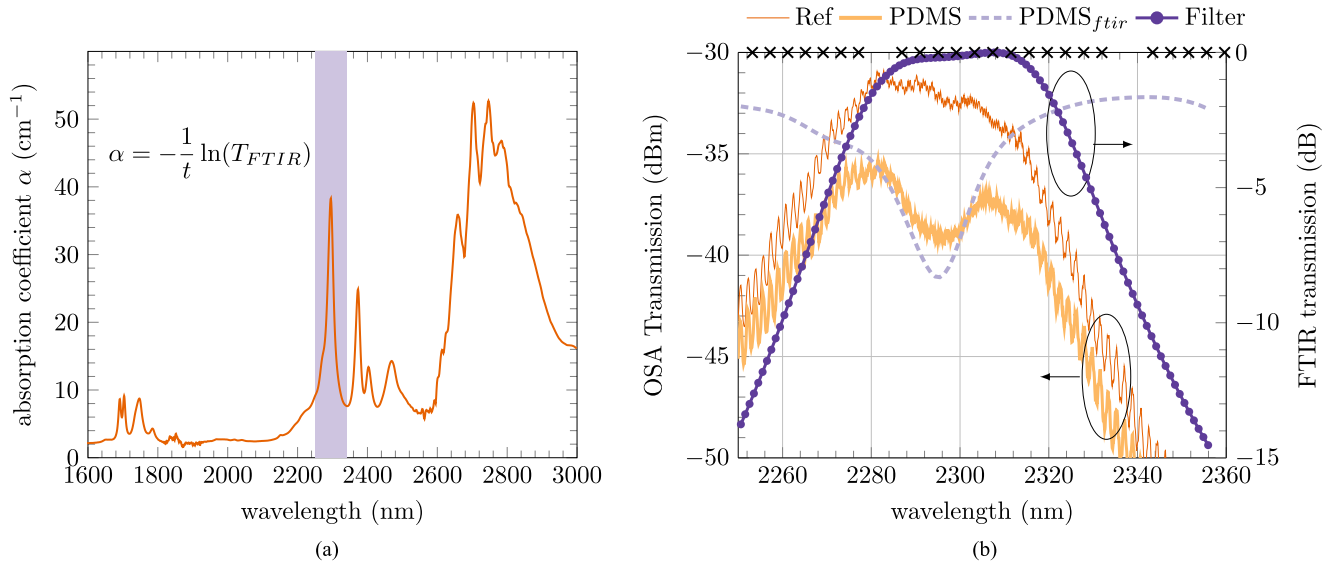

Fig. 4. The absorption coefficient of PDMS in the near- to mid-infrared wavelength region is estimated by using the Lambert-Beer law and the FTIR transmission spectrum of a ($t = 0.5$ mm) thick PDMS foil (a). The wavelength region for the absorption spectroscopy experiment is colored. After passing the bandpass filter, see Fig. 1(a), the optical spectrum coupled into the fiber is measured using the Yokogawa OSA: in the case when PDMS is present (PDMS) and when it is removed (Ref) (b). The measured total optical power is 11.5 μW and 31.4 μW, respectively. The normalized FTIR transmission of the PDMS sample (PDMS$_{ftir}$) and the bandpass (Filter) is also shown. The black crosses on the top axis show the AWG peak wavelengths. Ideally, the AWG response would be limited to within one FSR closest to the PDMS absorption feature. The filter is centered at 2305 nm with a FWHM of 50 nm and overlaps unintentionally with the next FSR on the blue side of the PDMS absorption peak. As a result, the longer wavelength channels of the AWG spectrometer will show additional crosstalk.

The combined output from the channels of the AWG results in a PD signal of 3.7 V for the reference measurement and 1.4 V when PDMS is introduced. The optical power inside each channel can be recovered by modulating each channel time-sequentially [34]. The modulation depth of the heaters is chosen such that it corresponds closely to a π-phase shift of each MZI.

Slight differences in fabrication lead to drive voltages V_π that are spread between 6 and 7 V and the corresponding switching power varies between 48–56 mW. An example of modulation of one such channel is shown in Fig. 5(a). For each heater bias point, four consecutive PD value are collected and averaged. The PD output is collected for 1 second for each channel
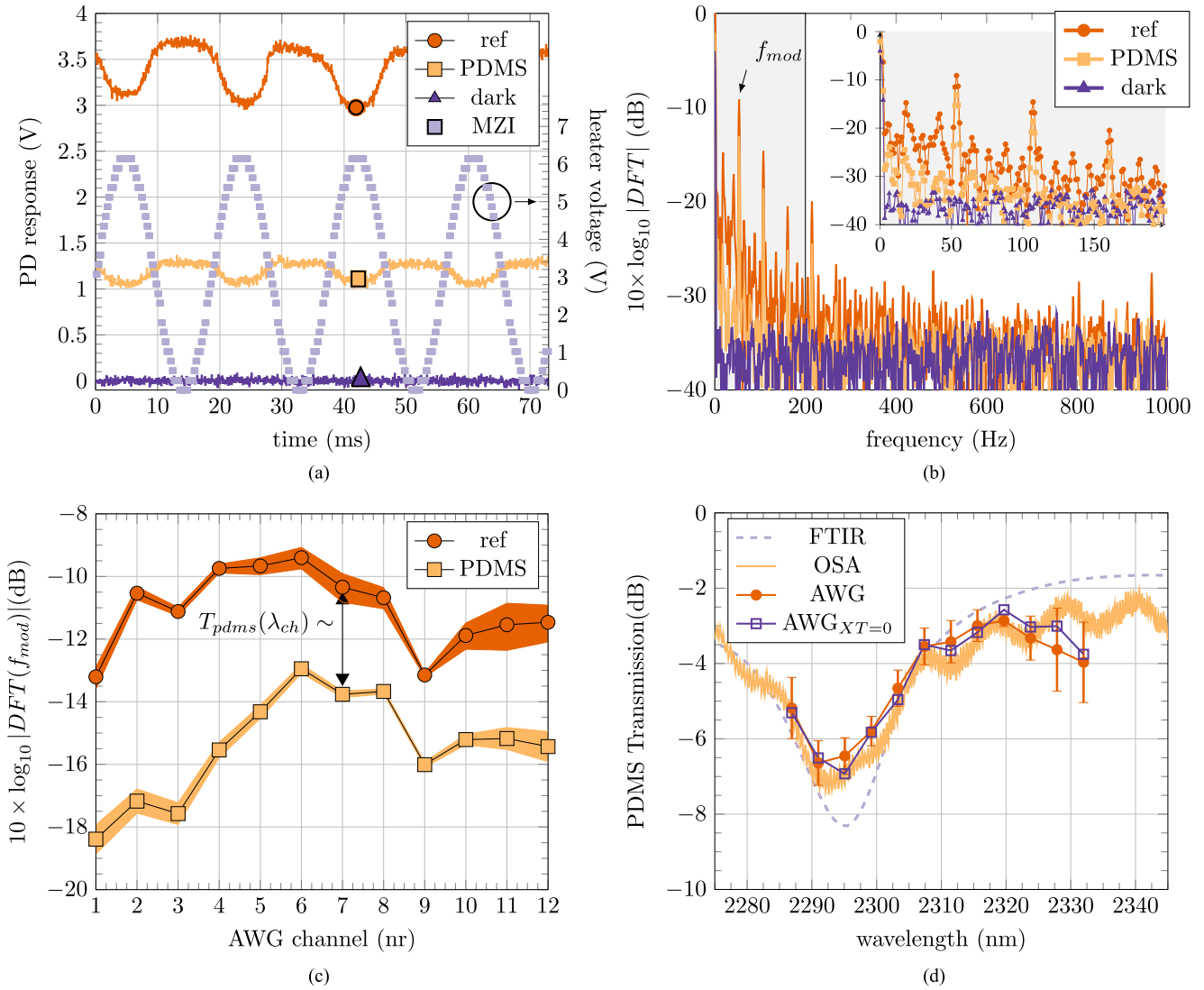
Fig. 5. Response of the photodiode to a sinusoidal modulation of one AWG channel. The first thousand sample points are shown for three cases: prior to the chip, the light passes through a 0.5 mm thick PDMS sheet, a reference measurement without PDMS and a dark measurement without the light source (a). The sample points are collected by a microcontroller in packets and are not linked to an external clock. The resulting PD sampling rate is ≈24 kSa/s. The time intervals between samples can be slightly different and the given time axis is an appproximation. For each setpoint of the heater, four consecutive PD readings are collected. The logarithmic DFT spectrum of the PD response is shown (b). The difference in maxima between the 'PDMS' and 'ref' measurement at the modulation frequency f_{mod} is used to determine the spectral response of PDMS at the peak wavelength of each AWG channel (c). The colored region boundaries are the $\mu \pm \sigma$ values for seven different measurements. The optical modulation depth difference of the PD between the PDMS and reference measurement is plotted for each AWG channel with the corresponding channel peak wavelength (d). The results agree well with the results obtained by measuring the PDMS transmission using the benchmark mid-IR Yokogawa OSA. Main cause of variation is power and alignment drift of the source to the spectrometer. Taking the OSA spectrum as the true response of PDMS in this setup, calculations show that an idealized AWG with zero crosstalk XT would produce almost identical results.

consecutively with a sampling rate of 24 kSa/s. This corresponds to the response to 50 sinusoidal heating cycles for each channel. After sweeping the twelve channnels of the AWG, the discrete Fourier Transform (DFT) of the signal is performed on the four-piece averaged output using the fast-fourier transform (FFT) algorithm with a Kaiser smoothing window. The result for one channel is shown in Fig. 5(b). The absolute value of the DFT spectrum at the modulation frequency is proportional to the optical power modulation of that channel. This value is obtained for each of the twelve channels for the case when there is no PDMS in the free space beam path and when it is introduced, see Fig. 5(c). The difference between the two is a measure for

the absorption spectrum of PDMS, sampled at the peak wavelengths of the AWG channels. The colored region boundaries are the $\mu \pm \sigma$ values for seven different measurements where the main cause of variation is power and alignment drift of the source to the spectrometer. The absorption spectrum of PDMS obtained in this manner corresponds well to the OSA benchmark measurement, see Fig. 5(d). A slight discrepancy for the longer wavelength channels is observed as expected. This is due to the fact that the central wavelength of the bandpass filter is not exactly centered to one FSR of the AWG, see Fig. 4(b). Taking the OSA spectrum as the true response of PDMS in this setup, calculations show that an idealized AWG with zero crosstalk

and insertion loss would produce almost identical results. The idealized AWG is taken as an array of dirac functions at the AWG channel peak positions, see black crosses in Fig. 4(b).

The Signal-to-Noise Ratio (SNR) for each channel of the system is found by comparing the signal strength at the modulation frequency in the reference measurement with the noise power in dark conditions at f_{mod}, see Fig. 5(b). The SNR is between 24–28 dB for 1s integration time per channel. Using the input optical power spectrum from Fig. 4(b) and the SNR for each channel, it is estimated that the lowest power change ΔP that can be detected (with SNR = 1) is between -57.2 dBm/nm and -69.2 dBm/nm. For a given spectroscopic application where one would want to detect a minimum transmission change ΔT of 0.1% (-30 dB) with SNR = 1, a broadband source with a minimum power density of -27.2 dBm/nm or a total power of -10 dBm within one FSR (50 nm) is required . Although these values are adequate for most applications, there are several ways to further improve the performance of the device.

The detectivity of the photodetector can be increased by active cooling or by using an optical immersion microlens [35]. The input grating coupler can be replaced with a spot-size converter for edge-coupling for higher efficiency and larger optical bandwidth. Moreover, the input fiber should be fixed to avoid drift of the coupling efficiency to the spectrometer during the measurement. The channels can be addressed simultaneously at a different modulation frequency instead of time-sequentially, thus increasing the measurement time per channel, thereby increasing SNR. For testing purposes, the output grating coupler array in this design is sized to match the mode field diameter of the single-mode fibers. However, the array can be readily shrunk ten-fold for better collection efficiency or to allow for more output channels.

Finally for applications where large environmental temperature variations are present, the central wavelength of the device will shift by ≈ 0.125 nm/K at 2.3 μm wavelength, resulting in a small offset of the wavelength corresponding with each channel. To mitigate this, one can either use a temperature controller underneath the photonic chip, use specially designed athermal circuits [36] or use SiN waveguide circuits with a five times lower thermo-optic coefficient [37].

V. CONCLUSION

Low-cost and miniaturized spectrometers can be realized by combining an off-the-shelf mid-infrared photodetector with SOI wavelength demultiplexer circuits. A novel approach is shown where a single discrete photodetector is used to characterize the response of a twelve channel mid-infrared AWG at 2.3 μm. The different AWG channels are discerned by time-sequentially modulating the output arms with MZI-based thermo-optic modulators. The driving and read-out of the spectrometer is performed using low-cost standard electronic components. The absorption spectrum of PDMS is recovered at 2.3 μm to good agreement with bench-top OSA measurements. This is a promising approach which can be applied to longer wavelength SOI spectrometers for the 3–4 μm wavelength range where high-performance cooled detectors are needed.

REFERENCES

[1] R. Soref, "The past, present, and future of silicon photonics," *IEEE J. Sel. Topics Quantum Electron.*, vol. 12, no. 6, pp. 1678–1687, Nov. 2006.

[2] M. Pantouvaki *et al.*, "Active components for 50 Gb/s NRZ-OOK optical interconnects in a silicon photonics platform," *J. Lightw. Technol.*, vol. 35, no. 4, pp. 631–638, Apr. 2017.

[3] M. H. Khan *et al.*, "Ultrabroad-bandwidth arbitrary radiofrequency waveform generation with a silicon photonic chip-based spectral shaper," *Nature Photon.*, vol. 4, no. 2, pp. 117–122, Feb. 2010.

[4] A. Abbasi *et al.*, "III-V-on-Silicon C-band high-speed electro-absorption modulated DFB laser," *J. Lightw. Technol.*, vol. 36, no. 2, pp. 252–257, Aug. 2017.

[5] A. E.-J. Lim *et al.*, "Review of silicon photonics foundry efforts," *IEEE J. Sel. Top. Quantum Electron.*, vol. 20, no. 4, pp. 405–416, Jul. 2014.

[6] J. T. Kindt, M. S. Luchansky, A. J. Qavi, S.-H. Lee, and R. C. Bailey, "Subpicogram per milliliter detection of interleukins using silicon photonic microring resonators and an enzymatic signal enhancement strategy," *Anal. Chem.*, vol. 85, no. 22, pp. 10 653–10 657, Nov. 2013.

[7] E. Ryckeboer, R. Bockstaele, M. Vanslembrouck, and R. Baets, "Glucose sensing by waveguide-based absorption spectroscopy on a silicon chip," *Biomed. Opt. Express*, vol. 5, no. 5, pp. 1636–1648, May 2014.

[8] Y. Chen, H. Lin, J. Hu, and M. Li, "Heterogeneously integrated silicon photonics for the mid-infrared and spectroscopic sensing," *ACS Nano*, vol. 8, no. 7, pp. 6955–6961, Jun. 2014.

[9] Y. Li, P. Segers, J. Dirckx, and R. Baets, "On-chip laser Doppler vibrometer for arterial pulse wave velocity measurement," *Biomed. Opt. Express*, vol. 4, no. 7, pp. 1229–1235, Jul. 2013.

[10] H. Yan *et al.*, "Specific detection of antibiotics by silicon-on-chip photonic crystal biosensor arrays," *IEEE Sens. J.*, vol. 17, no. 18, pp. 5915–5919, Sep. 2017.

[11] Y. E. Marin, T. Nannipieri, C. J. Oton, and F. Di Pasquale, "Integrated FBG sensors interrogation using active phase demodulation on a silicon photonic platform," *J. Lightw. Technol.*, vol. 35, no. 16, pp. 3374–3379, Aug. 2017.

[12] A. Trita *et al.*, "Simultaneous interrogation of multiple fiber Bragg grating sensors using an arrayed waveguide grating filter fabricated in SOI platform," *IEEE Photon. J.*, vol. 7, no. 6, Dec. 2015, Art. no. 7802611.

[13] T. H. Stievater *et al.*, "Trace gas absorption spectroscopy using functionalized microring resonators," *Opt. Lett.*, vol. 39, no. 4, pp. 969–972, Feb. 2014.

[14] N. A. Yebo *et al.*, "Selective and reversible ammonia gas detection with nanoporous film functionalized silicon photonic micro-ring resonator," *Opt. Express*, vol. 20, no. 11, pp. 11 855–11 862, May 2012.

[15] P. Larkin, *Infrared and Raman Spectroscopy; Principles and Spectral Interpretation*. New York, NY, USA: Elsevier, 2011.

[16] R. Soref, "Mid-infrared photonics in silicon and germanium," *Nature Photon.*, vol. 4, no. 8, pp. 495–497, Aug. 2010.

[17] G. Roelkens *et al.*, "Silicon-based heterogeneous photonic integrated circuits for the mid-infrared," *Opt. Mater. Express*, vol. 3, no. 9, pp. 1523–1536, Sep. 2013.

[18] G. Z. Mashanovich *et al.*, "Silicon photonic waveguides and devices for near- and mid-IR applications," *IEEE J. Sel. Top. Quantum Electron.*, vol. 21, no. 4, Jul. 2015, Art. no. 8200112.

[19] R. Wang *et al.*, "III-V-on-silicon photonic integrated circuits for spectroscopic sensing in the 2–4 μm wavelength range," *Sensors*, vol. 17, no. 8, p. 1788, Aug. 2017.

[20] J. S. Penadés *et al.*, "Suspended silicon mid-infrared waveguide devices with subwavelength grating metamaterial cladding," *Opt. Express*, vol. 24, no. 20, pp. 22908–22916, Oct. 2016.

[21] S. A. O. Miller, "Low-loss silicon platform for broadband mid-infrared photonics," *Optica*, vol. 4, no. 7, pp. 707–712, Jul. 2017.

[22] B. G. Lee *et al.*, "DFB quantum cascade laser arrays," *IEEE J. Quantum Electron.*, vol. 45, no. 5, pp. 554–565, May 2009.

[23] A. Spott *et al.*, "Quantum cascade laser on silicon," *Optica*, vol. 3, no. 5, pp. 545–551, May 2016.

[24] L. Bizet *et al.*, "Multi-gas sensing with quantum cascade laser array in the mid-infrared region," *Appl. Phys. B*, vol. 123, no. 5, p. 145, May 2017.

[25] R. Wang *et al.*, "Broad wavelength coverage 2.3 μm III-V-on-silicon DFB laser array," *Optica*, vol. 4, no. 8, pp. 972–975, Aug. 2017.

[26] P. Barritault *et al.*, "Design, fabrication and characterization of an AWG at 4.5 μm," *Opt. Express*, vol. 23, no. 20, pp. 26168–26181, Oct. 2015.

[27] A. Vasiliev, M. Muneeb, R. Baets, and G. Roelkens, "High resolution silicon-on-insulator mid-infrared spectrometers operating at 3.3 μm," in *Proc. IEEE Photon. Soc. Summ. Top. Meeting Ser.* Jul. 2017, pp. 177–178.

[28] M. Nedeljkovic *et al.*, "Mid-infrared silicon-on-insulator Fourier-transform spectrometer chip," *IEEE Photon. Technol. Lett.*, vol. 28, no. 4, pp. 528–531, Feb. 2016.

[29] M. Erfan *et al.*, "On-chip micro–electro–mechanical system fourier transform infrared (MEMS FT-IR) spectrometer-based gas sensing," *Appl. Spectr.*, vol. 70, no. 5, pp. 897–904, May 2016.

[30] X. Nie, E. Ryckeboer, G. Roelkens, and R. Baets, "CMOS-compatible broadband co-propagative stationary Fourier transform spectrometer integrated on a silicon nitride photonics platform," *Opt. Express*, vol. 25, no. 8, pp. A409–A418, Apr. 2017.

[31] M. Muneeb *et al.*, "III-V-on-silicon integrated micro – spectrometer for the 3 μm wavelength range," *Opt. Express*, vol. 24, no. 9, pp. 9465–9472, May 2016.

[32] P. Munoz, D. Pastor, and J. Capmany, "Modeling and design of arrayed waveguide gratings," *J. Lightw. Technol.*, vol. 20, no. 4, pp. 661–674, Apr. 2002.

[33] R. Wang *et al.*, "III-V-on-silicon 2-μm-wavelength-range wavelength demultiplexers with heterogeneously integrated InP-based type-II photodetectors," *Optics Express*, vol. 24, no. 8, pp. 8480–8490, 2016.

[34] R. Baets, D. Delbeke, G. Roelkens, and W. Bogaerts, "Integrated spectrometers with single pixel detector," U.S. Patent App. 15/305,713, Mar. 23, 2017.

[35] J. Piotrowski, W. Galus, and M. Grudzien, "Near room-temperature ir photo-detectors," *Infrared Phys.*, vol. 31, no. 1, pp. 1–48, 1991.

[36] L. Wang *et al.*, "A thermal arrayed waveguide gratings in silicon-on-insulator by overlaying a polymer cladding on narrowed arrayed waveguides," *Appl. Opt.*, vol. 51, no. 9, pp. 1251–1256, 2012.

[37] P. T. Lin *et al.*, "Low-stress silicon nitride platform for mid-infrared broadband and monolithically integrated microphotonics," *Adv. Opt. Mat.*, vol. 1, no. 10, pp. 732–739, 2013.

Jeroen Allaert received the M.Sc. degree in electronics with specialization in design techniques in 2006 from the University College Ghent, Ghent, Belgium. He was with the Photonics Research Group, Ghent University, Ghent, Belgium, from 2006 to 2017. He founded and is currently with the Analogue Renaissance, a company specialized in electronics for musical purposes and custom design, which was incorporated as Cask Strength Electronics in 2016.

Joris Van Campenhout received the Masters degree in physics engineering, in 2002, and the Ph.D. degree in electrical engineering, in 2007, both from Ghent University, Ghent, Belgium. After his Ph.D., he worked as a Postdoctoral Researcher with the IBM T. J. Watson Research Center, New York, NY, USA. In 2010, he joined IMEC, Belgium, where he is currently the Program Manager Optical I/O.

Roel Baets (F'07) received the M.Sc. degree in electrical engineering from Ghent University (UGent), Ghent, Belgium, in 1980, the second M.Sc. degree from Stanford University, Stanford, CA, USA, in 1981, and the Ph.D. degree from UGent, in 1984. He is a Full Professor with UGent and is associated with the IMEC. From 1984 to 1989, he held a Postdoctoral position with IMEC. Since 1989, he has been a Professor with the Faculty of Engineering and Architecture, UGent, where he founded the Photonics Research Group. From 1990 to 1994, he was a part-time Professor with Delft University of Technology and from 2004 to 2008, with Eindhoven University of Technology. He has mainly worked in the field of integrated photonics. As part of a team of eight professors Roel Baets leads the Photonics Research Group. In 2006, he founded the ePIXfab, the globally first multiproject-wafer service for silicon photonics. Since then ePIXfab has evolved to become the European Silicon Photonics Alliance. He is also the Director of the multidisciplinary Center for Nano- and Biophotonics (NB Photonics) at UGent, founded in 2010. He was a cofounder of the European M.Sc. programme in Photonics. Roel Baets is an ERC grantee of the European Research Councile and a Methusalem grantee of the Flemish government. He is a Fellow of the European Optical Society and Optical Society. He is also a member of the Royal Flemish Academy of Belgium for Sciences and the Arts.

Anton Vasiliev received the B.Sc. degree in applied physics engineering in 2012, and the M.Sc. degree in photonics in 2014 from Ghent University, Ghent, Belgium. He is currently working toward the Ph.D. degree in photonics with the Photonics Research Group, Department of Information Technology, IMEC, Ghent University, Ghent, Belgium. His current research interests include integrated circuits on SOI platform for mid-infrared spectroscopy applications and photothermal methods for trace gas detection. He is a member of the IEEE Photonics Society and the OSA Optical Society.

Muhammad Muneeb was born in 1982 in Pakistan. He received the B.Sc. degree in electronic engineering from the GIK Institute of Engineering and Technology, Topi, Pakistan, in 2005, and the Erasmus Mundus Masters degree in photonics from the Royal Institute of Technology, Stockholm, Sweden and Ghent University, Ghent, Belgium, in 2010. Since November 2010, he has been with the Photonics Research Group, Ghent University, where his research focus is on IIIV/Si photonic circuits for mid-infrared spectroscopic applications.

Günther Roelkens received the degree in electrical engineering and the Ph.D. degree from Department of Information Technology (INTEC), Ghent University, Ghent, Belgium, in 2002 and 2007, respectively, where he is currently an Associate Professor. In 2008, he was a Visiting Scientist with the IBM T. J. Watson Research Center, Rochester, NY, USA. He is an Assistant Professor with Eindhoven University of Technology, Eindhoven, The Netherlands. His research interests include the heterogeneous integration of III-V semiconductors and other materials on top of silicon waveguide circuits and electronic/photonic cointegration. He was holder of an ERC starting grant (MIRACLE), to start up research in the field of integrated mid-infrared photonic integrated circuits.